

# Dynamic recrystallisation can produce porosity in shear zones

James Gilgannon<sup>1</sup>, Thomas Poulet<sup>2,3</sup>, Alfons Berger<sup>1</sup>, Auke Barnhoorn<sup>4</sup>,  
Marco Herwegh<sup>1</sup>

<sup>1</sup>Institute of Geological Sciences, University of Bern, Baltzerstrasse 1+3, 3012 Bern, Switzerland

<sup>2</sup>CSIRO Mineral Resources, Kensington, WA 6151, Australia

<sup>3</sup>School of Minerals and Energy Resources Engineering, UNSW Sydney, NSW 2052, Australia

<sup>4</sup>Department of Geoscience and Engineering, Delft University of Technology, Delft, The Netherlands

## Key Points:

- Creep cavities emerge with grain-size reduction by sub-grain rotation recrystallisation.
- Porosity driven by creep can be opened and sustained at high confining pressures.
- There is a direct and spontaneous physical path for single phase rocks to transition to polyphase rocks during deformation.

---

Corresponding author: James Gilgannon, [james.gilgannon@geo.unibe.ch](mailto:james.gilgannon@geo.unibe.ch)

## 15 Abstract

16 Creep cavities are increasingly recognised as an important syn-kinematic feature  
 17 of shear zones but much about this porosity needs investigation. Largely, observations  
 18 of creep cavities are restricted to very fine grained mature ultramylonites and it is un-  
 19 clear when they developed during deformation. Specifically, a question that needs test-  
 20 ing is; *should grain-size reduction during deformation produce creep cavities?* To this end,  
 21 we have reanalysed the microstructure of a large shear strain laboratory experiment that  
 22 captures grain-size change by dynamic recrystallisation during mylonitisation. We find  
 23 that the experiment does contain creep cavities. Using a combination of scanning elec-  
 24 tron microscopy and spatial point statistics, we show that creep cavities emerge with,  
 25 and because of, sub-grain rotation recrystallisation during ultramylonite formation. As  
 26 dynamic recrystallisation is ubiquitous in natural shear zones, this observation has im-  
 27 portant implications for the interpretation of concepts such as the Goetze criterion, palaeopiezome-  
 28 tery and phase mixing.

## 29 Plain Language Summary

30 At great depths inside the Earth, rocks called mylonites slowly deform and accom-  
 31 modate tectonic forces. Generally, these rocks are considered to have no porosity because  
 32 the pressure they experience is very large. However, it is frequently documented that these  
 33 mylonites focus the transport of mass, both fluid and solid, through the Crust. This im-  
 34 plies that mylonites host a permeable porosity. To better understand this paradox, we  
 35 reanalysed an old laboratory experiment that documented the formation of a mylonite.  
 36 We showed that a porosity, known as creep cavities, forms synchronously with the my-  
 37 lonite. This is an important experimental finding because it suggests that creep cavities  
 38 are a fundamental feature of mylonites. Our results showcase a rare snapshot into the  
 39 dynamics of rocks important for tectonics and advance larger questions about their trans-  
 40 port properties.

## 41 1 Introduction

42 Shear zones have long been recognised as important because they mechanically re-  
 43 lease tectonic stresses and focus the transport of mass, both fluid and solid, through the  
 44 Earth. Recently, it has been argued that mature fine grained polymineralic shear zones  
 45 host a permeable porosity known as creep cavities (Dimanov et al., 2007; Fousseis et al.,  
 46 2009) and that the processes of creep cavitation facilitates the migration of fluid and aids  
 47 dissolution and precipitation processes (Herwegh & Jenni, 2001). This new paradigm has  
 48 cast the discussion of deep fine grained fault rocks away from classical kinematics and  
 49 into a new more dynamic light. Field and experimental studies on creep cavities have  
 50 provided new context to the long discussed problems of phase mixing in ultramylonites  
 51 (Dimanov et al., 2007; Menegon et al., 2015; Précigout & Stünitz, 2016; Gilgannon et  
 52 al., 2017; Lopez-Sanchez & Llana-Fúnez, 2018) and advection driven fluid and mass trans-  
 53 fer in shear zones (Fousseis et al., 2009; Menegon et al., 2015; Précigout et al., 2017, 2019).  
 54 Beyond this there are many questions that need to be addressed to correctly place creep  
 55 cavities within the geological framework of large-scale shear zones.

56 First among these is what specific factors promote or inhibit creep cavity forma-  
 57 tion in rocks? A critical assumption in most of the work on creep cavities has been that  
 58 a grain-size sensitive rheology is needed for their formation. For example, in natural shear  
 59 zones microstructural evidence has been presented to argue that creep cavities emerge  
 60 with the production of fine grained mixtures during symplectite reactions and the tran-  
 61 sition to a grain-size sensitive rheology (Ceccato et al., 2018). Additionally, creep cav-  
 62 ities have been interpreted to become active after fracture induced grain-size reduction  
 63 of feldspar in granulite rocks (Menegon et al., 2013). This would seem to place a limit

64 on the activity of creep cavitation and presents a test for its emergence. More generally,  
 65 this could suggest that *any syn-kinematic grain-size reducing process inside of a ductile*  
 66 *shear zone has the potential to produce creep cavities.*

67 Dynamic recrystallisation is a major grain-size reduction mechanism in shear zones  
 68 and it is observed or interpreted for almost all of Earth's major constitutive minerals (for  
 69 example: calcite (Ter Heege et al., 2002; Bestmann & Prior, 2003); quartz (Hirth & Tullis,  
 70 1992; Stipp et al., 2002); feldspar (Tullis & Yund, 1985; Kruse et al., 2001); olivine (Lee  
 71 et al., 2002; Michibayashi et al., 2006). As dynamic recrystallisation is ubiquitous in shear  
 72 zones, any porosity produced as a consequence could play an important role in large-scale  
 73 shear zone processes. Here we revisit confined experiments that documented the process  
 74 of grain-size reduction by dynamic recrystallisation at high homologous temperatures  
 75 for Carrara marble. We use these experiments to test the hypothesis that dynamic re-  
 76 recrystallisation by sub-grain rotation should produce creep cavities. In a calculated rep-  
 77 resentative microstructure, we show statistically that dynamic recrystallisation does in-  
 78 deed generate a syn-kinematic porosity and discuss some of the consequences of this new  
 79 finding.

## 80 2 Materials and Methods

81 We revisit the Carrara Marble sample P0422 from the high shear strain torsion ex-  
 82 periments of Barnhoorn et al. (2004) (fig. 1a). The sample was deformed to a shear strain  
 83 ( $\gamma$ ) of 5 with a constant shear strain rate ( $\dot{\gamma} = 3 \times 10^{-4}$ ) at a temperature of 1000K and  
 84 a confining pressure of 300 MPa (Text S1). Specifically, this sample captures pervasive,  
 85 but incomplete, microstructural change through dynamic recrystallisation by sub-grain  
 86 rotation recrystallisation (fig. 1b). In addition to this we observe a previously unreported  
 87 grain boundary porosity (fig. 1c and d). We utilise the window this sample provides into  
 88 the deformation dynamics to evaluate any relationship between syn-kinematic pores and  
 89 newly recrystallised grains.

90 We analyse a close to tangential cut from the cylindrical sample. This cut approx-  
 91 imately corresponds to the XZ plane of finite strain and captures close to the maximum  
 92 shear strain and shear strain rate of the deformed sample (Paterson & Olgaard, 2000).

93 The main results of this contribution come from sample PO422 but we find sup-  
 94 porting evidence for syn-kinematic grain boundary porosity in two more samples that  
 95 have experienced both more shear strain and recrystallisation. The samples are PO274  
 96 ( $\dot{\gamma} = 3 \times 10^{-4}$ ,  $\gamma = 6.9$ ) and PO303 ( $\dot{\gamma} = 1 \times 10^{-3}$ ,  $\gamma = 7.9$ ). We have provided addi-  
 97 tional, more qualitative, information about these experiments along side our criteria for  
 98 defining the porosity as syn-kinematic in Text S2.

### 99 2.1 Defining a representative microstructure

100 To meaningfully assess any relationships between microstructural components we  
 101 calculated a 2D representative volume element (RVE). The RVE defines the minimum  
 102 area required to capture any variation in the microstructure (cf. Akker et al., 2018). This  
 103 is achieved by expanding the area of investigation until the feature of interest, in our case  
 104 porosity, stops varying. We borrow this homogenisation approach from the calculation  
 105 of material properties, like the elastic moduli, where the RVE provides a minimum sam-  
 106 ple size that can accurately describe the property (Hill, 1963; Regenauer-Lieb et al., 2014).

107 Using a large (4.2 x 3.8 mm on a scale of 1:0.55; px :  $\mu m$ ) backscatter electron (BSE)  
 108 mosaic (fig. 1a) segmented for porosity, the RVE was obtained by randomly generating  
 109 a series of increasingly larger boxes across the sample and then calculating the poros-  
 110 ity contained within (fig. 2a). This procedure was repeated 100 times to give statisti-  
 111 cally robust distributions for each box size. The change in standard deviation with box

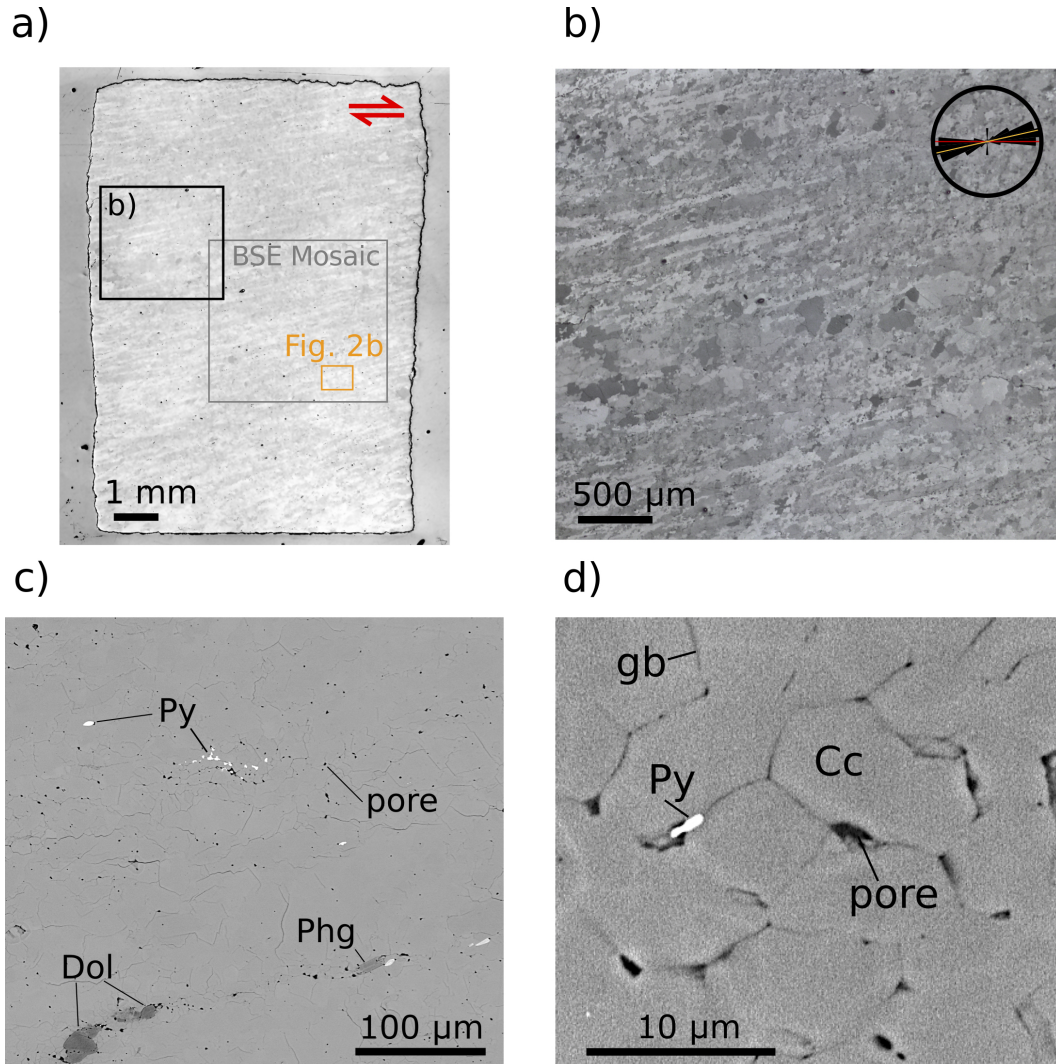


**Figure 1.** An overview of the investigated section and the details of its microstructures: a) shows a reflected light image of the cut section with the areas of analysis highlighted; b) is a reflected light image of the microstructure with an inset rose diagram of the long axis orientations of 83 phengite minerals. The red and orange lines in the rose diagram are the shear plane and the calculated angular shear for  $\gamma = 5$  (see Text S7); c) and d) are backscatter electron images that document the new observation of creep cavities in the experiment. (Py = pyrite, Dol = dolomite, Phg = phengite, Cc = calcite, gb = grain boundary)



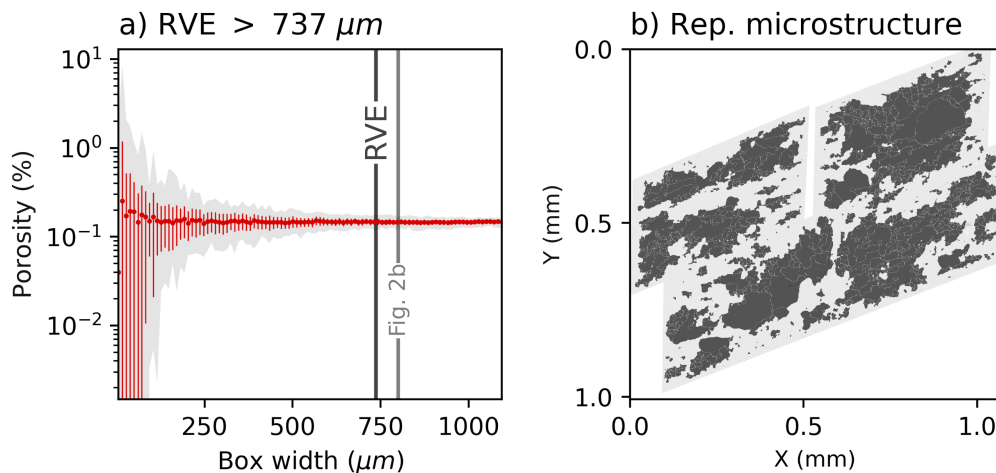


**Figure 2.** A visualisation of the calculated threshold for defining the representative microstructure (fig. 2a) and the mapped representative microstructure (fig. 2b) (for details see section 2.1). In figure 2a the red dot, red lines and the grey shaded area represent the mean,  $\pm 1$  standard deviation of the distribution and the maximum/minimum envelope respectively. Figure 2b shows the BSE and EBSD grain maps of the representative microstructure on top of one another.

112 size is used to determine the RVE because it best reflects a decrease in the variation of  
 113 the calculation (Figure S1). For perspective, the area of the mosaic used for the RVE  
 114 calculation is approximately equal to 19% of the area of the tangential cut shown in fig-  
 115 ure 1a. Once the minimum area needed was identified (fig. 2a), a set of electron backscat-  
 116 ter diffraction (EBSD) maps and a local BSE map were made on a representative mi-  
 117 crostructure (fig. 2b).

118 Details about the acquisition and processing of data is reported in the supplement.

## 119 2.2 Statistical analysis of pores and grains in space

120 On this representative microstructure we employed spatial point statistics to test  
 121 the spatial relationships between the observed porosity and different grain-size popula-  
 122 tions. Importantly, when this statistical information is combined with knowledge of the  
 123 deformation path and active processes a causal model of pore formation can be formul-  
 124 ated.

125 First, the spatial coincidence of the different data sets needed to be assured. To  
 126 achieve this, the EBSD output rasters were all mapped to the BSE map in QGIS with  
 127 the Georeferencer plugin. A thin plate spline transformation was used with a cubic spline  
 128 resampling on a total of 623 tie points between maps (Table S1). This process simulta-  
 129 neously corrected for distortions in the tilted EBSD data and ensured the correct spa-  
 130 tial positions of the data. Once corrected for distortion, the total area mapped by EBSD  
 131 approximates to  $650000 \mu\text{m}^2$ . In the context of the RVE calculation this value approx-  
 132 imately equates to an equivalent square box of  $800 \times 800 \mu\text{m}$  (fig. 2a).

133 From this corrected data set we extracted the centroids of pores and grains. As we  
 134 are interested in deformation induced changes in grain-size we chose to analyse two rel-  
 135 evant grain subsets: newly recrystallised grains ( $\leq 10 \mu\text{m}$ ) and relic grains ( $\geq 40 \mu\text{m}$ ).

136 For relic grains this corresponds to the smallest initial area-weighted grain-size reported  
 137 for the Carrara Marble by Pieri, Burlini, et al. (2001). For new grains the limit is cho-  
 138 sen to include the *steady state* grain-size reported by Barnhoorn et al. (2004) (6-10  $\mu\text{m}$ ).

139 To these subsets we applied the uni and bivariate forms of the pair correlation func-  
 140 tion (Wiegand et al., 2009; Wiegand & Moloney, 2014; Mitchell et al., 2015) in the soft-  
 141 ware Programita (Wiegand & Moloney, 2014). This spatial point analysis gives infor-  
 142 mation about the pair distances between points and how these data pairs are related in  
 143 space. More specifically, the pair correlation function describes how the true density func-  
 144 tion of the data compares to a density function of a spatially random model. Theoret-  
 145 ically, this means that pair correlation function values of 1 report that the data is dis-  
 146 tributed randomly in space, greater than 1 highlight spatial clustering, while values less  
 147 than 1 identify ordering, or anti-clustering. To account for the natural variation in real  
 148 data 199 simulations of randomness were calculated and provide an envelop for spatially  
 149 random data. The function is a non-cumulative statistic and is calculated for an expand-  
 150 ing radius of a ring with a specific width (Figure S7). This provides information about  
 151 the distances at which data points can ‘see’ other data points and if their relation is one  
 152 of clustering, ordering or randomness.

153 For the parameters used in the analysis please refer to the supplementary informa-  
 154 tion.

### 155 3 Results

#### 156 3.1 A general microstructural description

157 In general, the sample clearly shows a microstructural change from the starting grain-  
 158 size distribution (mean = 125  $\mu\text{m}$  (Barnhoorn et al., 2004)) to a new recrystallised grain-  
 159 size distribution (mean = 6-10  $\mu\text{m}$  (Barnhoorn et al., 2004)) (fig. 1). This change man-  
 160 ifests itself at the section scale and produces a foliation (fig. 1a). Upon closer inspec-  
 161 tion it can be seen that the foliation is made up of elongated calcite crystals (fig. 1b).  
 162 These elongated ribbon grains are plastically deformed and can be seen undergoing sub-  
 163 grain rotation recrystallisation to smaller grain-sizes (cf. Barnhoorn et al., 2004). Across  
 164 the sample the secondary phases are well distributed, with phengite showing orientations  
 165 that seem to track the foliation (see inset rose diagram in fig. 1b). The most striking fea-  
 166 ture in the sample is a conspicuous grain boundary porosity that can be qualitatively  
 167 associated to regions of finer grain-sizes (fig. 1c and d). The porosity is syn-kinematic,  
 168 a fact illustrated by the presence of precipitates forming in pores (fig. 1c and d), and we  
 169 interpret them as creep cavities (please refer to Text S2 for further criteria). We expect  
 170 these creep cavities to be filled with a fluid-gas mixture developed early in the exper-  
 171 iment from initial fluid inclusions and a  $\text{CO}_2$  partial pressure from decarbonation.

172 Three important microstructural elements are considered in the following: 1) *relic*  
 173 *grains* ( $\text{grains} \geq 40 \mu\text{m}$ ); 2) *newly recrystallised grains* ( $\text{grains} \leq 10 \mu\text{m}$ ); 3) *and creep*  
 174 *cavities*. The rest of the results will consider the relationship between these elements in  
 175 a calculated representative microstructure.

#### 176 3.2 Defining a representative microstructure

177 Using the method described in section 2.1, it was found that the minimum square  
 178 box size needed to describe a 2D representative volume element (RVE) is 737 x 737  $\mu\text{m}$   
 179 (fig. 2a).

180 The following results come from a series of analyses made on an area larger than  
 181 the calculated RVE (fig. 2a and b). This area is presented in figure 2b. and shows a BSE  
 182 map overlain by grain maps calculated from EBSD data. The grain-size distribution for  
 183 the representative microstructure highlights that microstructural change has not yet come

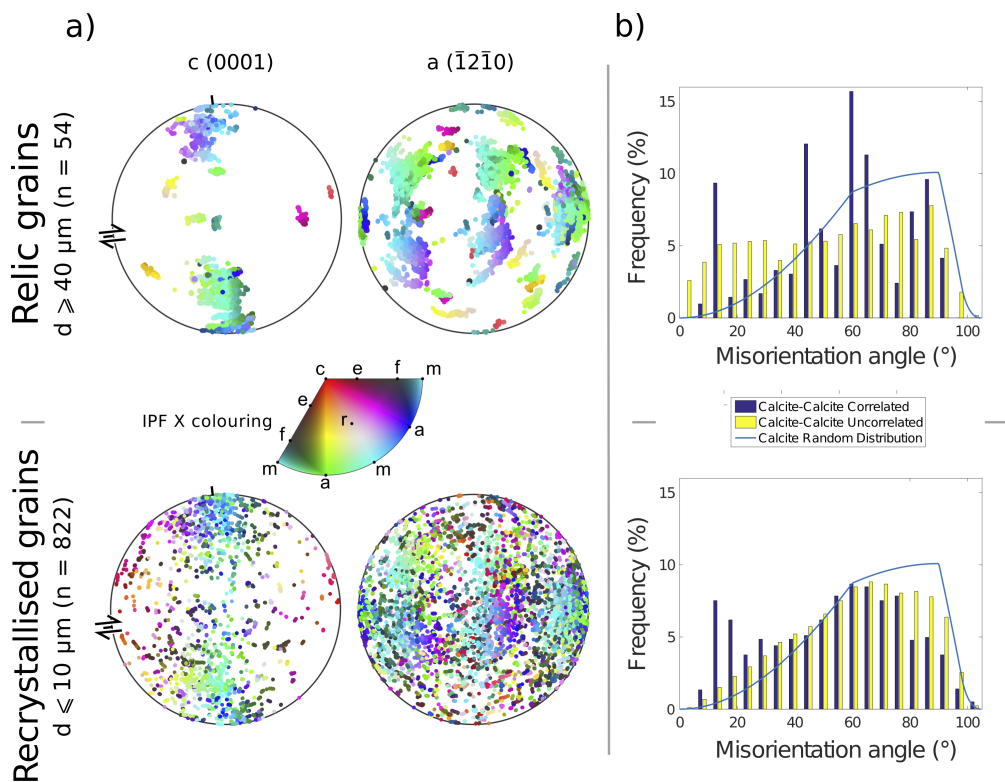


**Figure 3.** Visualisation of texture and orientations of the grain populations of interest. Figure 3a shows the *c*- and *a*-axis pole figures. 10000 random orientations are presented and coloured coded according to how their host grain’s crystallography is aligned with the X direction of finite strain. Figure 3b shows complementary grain misorientation histograms for both grain subsets. No sub-grain data is considered.

184 to completion but is well developed (Figure S6). The number weighted histogram of figure  
 185 S6 highlights the establishment of the peak identified by Barnhoorn et al. (2004) to  
 186 represent the *steady state* recrystallised grain-size of  $\approx 10 \mu\text{m}$ .

### 187 3.3 A representative texture

188 *Relic grains* show a clear crystallographic preferred orientation (CPO). There are  
 189 two major clusters in the *c*-axis pole figure (fig. 3a). This is reinforced by the inverse  
 190 pole figure colouring which highlights the same two dominant grain orientation sets found  
 191 by Barnhoorn et al. (2004) and Pieri, Kunze, et al. (2001). The misorientation histogram  
 192 for relic grains shows a distribution that is non-random for a hexagonal crystal system  
 193 (fig. 3b).

194 *Newly recrystallised grains* have a contrasting but complementary texture. The pole  
 195 figure data in figure (fig. 3a) shows a clear dispersion from the two dominant clusters  
 196 documented for the relic grains. However, it is clear from the inverse pole figure colouring  
 197 that grains retain an orientation that is close to the initial CPO of the relic grains.  
 198 The misorientation histogram for newly recrystallised grains indicates that grain orientations  
 199 are generally random but neighbouring grains retain lower relative misorientations  
 200 (fig. 3b).

### 201 **3.4 Spatial analysis of a representative microstructure**

202 The pair correlation function is used to understand the spatial distribution and relation-  
 203 ship between syn-kinematic pores, newly recrystallised grains and relic grains. For  
 204 this analyses a series of null hypotheses were defined. Broadly, these null hypotheses test  
 205 the geological question, is the syn-kinematic porosity generated randomly?

206 More specifically, we define three individual null hypotheses to test the spatial con-  
 207 figuration of 1) pores, 2) pores and newly recrystallised grains and 3) pores and relic grains.  
 208 For each of these null hypothesis we generate 199 simulations of randomly distributed  
 209 porosity. Additionally for the bivariant analyses, grains are fixed in space and the model  
 210 of randomness considers the spatial randomness of pores with respect to fixed grains. The  
 211 grey envelopes in each panel of figure 4 visualise the 5th largest and smallest simulation  
 212 of the 199 Monte Carlo simulations for the null hypotheses of each analysis.

#### 213 **3.4.1 Spatial distribution of pores**

214 Here we employ the univariant pair correlation function. Using the null hypoth-  
 215 esis that *pores are randomly distributed in space* we can see that the data does not con-  
 216 form to this model (fig. 4a). The analysis shows that data preferentially clusters at pair  
 217 distances between 1 and 30  $\mu m$ . There is also a weak divergence from the null model at  
 218 approximately 43  $\mu m$ . To better visualise the pair correlation result, figure 4d shows an  
 219 example pair distance between pore centres (e.g. blue line of 10  $\mu m$ ).

#### 220 **3.4.2 The relationship between pores and newly recrystallised grains**

221 In this case, we employ the bivariant pair correlation function. The null hypoth-  
 222 esis for randomness used here can be stated as: *pores are randomly distributed in space*  
 223 *with respect to newly recrystallised grains*. In this analysis the data does not conform to  
 224 the model of randomness (fig. 4b). Data is preferentially clustered at pair distances be-  
 225 tween 1 and 15  $\mu m$ . Figure 4d shows an example of pair distances between pore centres  
 226 and recrystallised grain centres (e.g. red line of 4  $\mu m$ ).

#### 227 **3.4.3 The relationship between pores and relic grains**

228 To test this relationship we again use the bivariant pair correlation function. The  
 229 modelled null hypothesis we test is that *pores are randomly distributed in space with re-*  
 230 *spect to relic grains*. The results show that the data does conform to this model (fig. 4c).  
 231 Pores and relic grains are randomly distributed in space with respect to one another.

## 232 **4 Interpretations and Discussion**

### 233 **4.1 Dynamic recrystallisation produces porosity**

234 Our microstructural textures document recrystallisation and, in line with the two  
 235 original experimental studies conducted on Carrara marble at the conditions revisited  
 236 (Pieri, Kunze, et al., 2001; Barnhoorn et al., 2004), we interpret the dominant mecha-  
 237 nism to be sub-grain rotation recrystallisation (Bestmann & Prior, 2003). Newly recryst-  
 238 tallised grains preserve aspects of their parent grain's texture. We choose to interpret  
 239 that an increased component of viscous grain boundary sliding allows for the randomi-  
 240 sation of the parent grains texture (fig. 3). We claim that a consequence of this increase  
 241 in viscous grain boundary sliding is the formation of creep cavities. The results presented  
 242 in figure 4 ratify this interpretation by documenting that pores and recrystallised grains  
 243 are clustered in space. Figure 4d summarises the relationship documented by the pair  
 244 correlation function. New pores are clustered in space and each pore is separated by dis-  
 245 tances approximately equal to the distribution of diameters of the recrystallised grain-

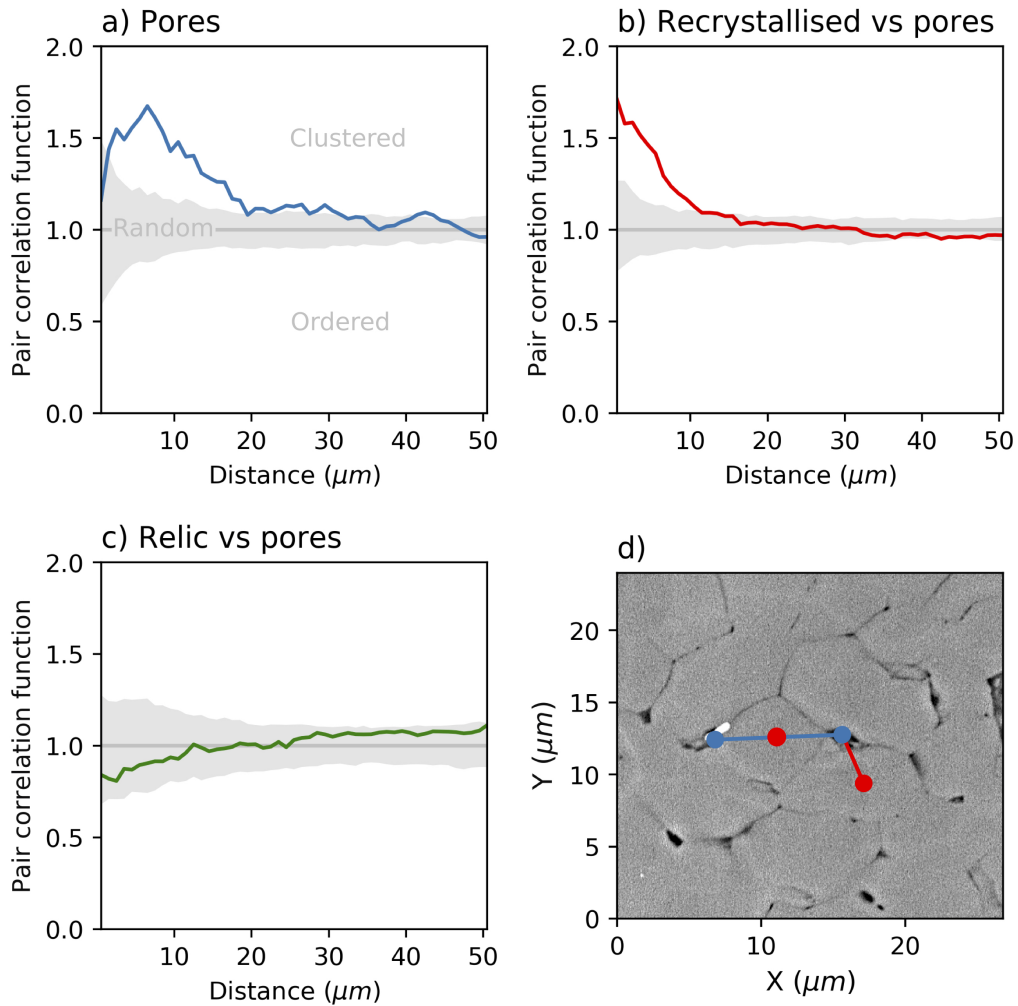


**Figure 4.** Spatial analysis of pores and grains. Figure 4a shows the univariate pair correlation analysis of pores, while figures 4b and c show the bivariate analysis. As highlighted in figure 4a, data falling within the grey envelope shows a spatially random distribution, data with values greater than this indicate clustering and data less than the random window is spatially ordered. Figure 5d summarises the results of figures 4a-c in a schematic way. See the text for details.



246 sizes (see example blue line in fig. 4d). While newly recrystallised grains are clustered  
 247 in space with pores at distances roughly half of the diameter of the recrystallised grain-  
 248 size (see example red line in fig. 4b). We suggest that the spatial relations of newly re-  
 249 crystallised grains and pores together with the EBSD data provide a statistical base to  
 250 the assertion that creep cavities emerge with, and because of, sub-grain rotation recryst-  
 251 tallisation.

## 252 4.2 The Goetze criterion

253 In the experiment we revisit the confining pressure ( $P_c = 300$  MPa) and the mean  
 254 stress ( $P_m = 319$  MPa) are roughly 5.3 and 5.6 times larger than the peak differential  
 255 stress ( $\sigma_{diff} = 57$  MPa) but despite this it is clear that dynamic recrystallisation pro-  
 256 duces an inter-granular porosity, creep cavities (fig. 1c and d). This is a significant ex-  
 257 perimental finding because it falsifies a common extension of the Goetze criterion; that  
 258 pores, driven by creep, will not open, and remain so, during a deformation where the con-  
 259 fining pressure is much larger than the differential stress (Evans & Kohlstedt, 1995; Mei  
 260 et al., 2010; Bercovici & Skemer, 2017).

261 Our findings do show that the absolute porosity percentage generated is small ( $\approx$   
 262 0.1 % (fig. 2a)), however its appearance is critically coupled with the process of dynamic  
 263 recrystallisation. This is very important because the porosity is not generated randomly  
 264 in space or time. The emergence of dynamic recrystallisation and creep cavitation can  
 265 then be said to be a part of the collective dissipative response of the material to the im-  
 266 posed deformation. Critically, this suggests that creep cavitation is a fundamental and  
 267 intrinsic thermo-mechanical dissipative process of a ductile fault rock. This interpreta-  
 268 tion, stated more plainly, emphasises that creep cavities are not an exotic feature of low  
 269 pressure experiments or synthetic samples but are a necessary micro-mechanical feature  
 270 of microstructural change during ductile creep.

271 This interpretation is not at odds with the Goetze criterion itself, which is a stress  
 272 condition ( $\sigma_1 - \sigma_3 = \sigma_{diff} = P$ ; eq. 16 in Evans and Kohlstedt (1995)) that empiri-  
 273 cally defines the brittle-ductile transition. Namely, in the revisited experiment, the ma-  
 274 terial has met its yield surface under the conditions of the Goetze criterion (more recently  
 275 stated by (Mei et al., 2010) as;  $\sigma_{diff} < P_m$ ). Importantly, the porosity phenomena de-  
 276 scribed in our results is a function of the proceeding irreversible deformation. Therefore,  
 277 while the magnitude of the principle stresses are an important initial condition for guar-  
 278 anteeing a ductile yielding, they do not predict the ultimate dissipative path of the ma-  
 279 terial.

## 280 4.3 Consequences for grain-size palaeopiezometry

281 If creep cavitation is a fundamental process of ductile grain refinement, this raises  
 282 several questions about the application of grain-size palaeopiezometry in monomineralic  
 283 aggregates. Broadly, this form of palaeopiezometry is based on the widespread empiri-  
 284 cal experimental observation that for monomineralic aggregates the differential stress  
 285 is inversely related to the average recrystallised grain or subgrain-size (see Twiss, 1977;  
 286 Austin & Evans, 2009; Hackl & Renner, 2013, & references therein). In detail, the em-  
 287 pirical observation is explained by several authors differently but can generally be sum-  
 288 marised to say that energetic gradients in the crystal lattice combined with grain surface  
 289 energy drive the establishment of a steady state grain-size. The specifics of each model  
 290 vary depending on which underlying recovery process is assumed to dominate but im-  
 291 portantly the base of all of the models is the empirical observation. Critically, an implicit  
 292 assumption in the all of the proposed theories of palaeopiezometry is that all grain-size  
 293 change is isochoric (De Bresser et al., 1998) and solely related to the distortions and re-  
 294 orienting of the crystal lattice. Porosity driven by creep is precluded and therefore so  
 295 is establishing grains by nucleation of new material in any dilatant sites. With the new

296 results presented here we can state that the implicit assumption of grain-size palaeopiezom-  
 297 etry in monomineralic aggregates may be incorrect.

298 Specifically, we have shown that pores do form with sub-grain rotation recrystallisation and have highlighted that at the very least second phases precipitate in the pores.  
 299 While it remains an open question whether or not calcite has also nucleated in some of  
 300 these sites, it is clear that pores allow for another path for a grain-size to be achieved.  
 301 Our evidence and reasoning agrees well with recent work by Précigout and Stünitz (2016),  
 302 where they interpreted that the olivine neoblasts nucleated and grew in creep cavities.  
 303 They argued this in part from evidence that a population of smaller ( $< 1 \mu\text{m}$ ) olivine  
 304 grains appear well distributed in the recrystallised aggregate (see fig. 6 in Précigout and  
 305 Stünitz (2016)). While Précigout and Stünitz (2016) do not provide direct evidence of  
 306 creep cavities, our results would support their assumption. Additionally in high shear  
 307 strain experiments on calcite-anhydrite mixtures, Cross and Skemer (2017) documented  
 308 that calcite grains with more anhydrite than calcite neighbours (phase boundary frac-  
 309 tion  $> 0.5$ ) had smaller grain sizes than predicted by the palaeopiezometry. This ob-  
 310 servation may only reflect the competition of grain boundary surface energy and pinning  
 311 processes of unlike phases but we would suggest it may highlight that the size of new grains  
 312 is governed by nucleation and growth. Taken together these three sets of high shear strain  
 313 experiments raise questions about where and when it would be valid to use grain-size  
 314 palaeopiezometry. In particular, our results pose a problem for the ubiquitous use of grain-  
 315 size palaeopiezometry in monomineralic domains of shear zones, like recrystallised quartz  
 316 ribbons, because it may mean that one cannot easily know how many of the measured  
 317 grains were in fact nucleated by precipitation rather than dynamically recrystallised. This  
 318 difficulty is further emphasised by recent evidence from natural shear zones that creep  
 319 cavities can form in monomineralic quartz aggregates (Gilgannon et al., 2017).  
 320

#### 321 4.4 Consequences for the paleowattmeter

322 Our findings also have implications for the paleowattmeter (Austin & Evans, 2009)  
 323 but they may be less problematic because its steady state grain-size is derived from a  
 324 rate of work equation. Fundamentally, the paleowattmeter proposes that a steady state  
 325 grain-size stabilises when there is a balance between the rate of grain-size reduction, driven  
 326 by the power stored in the microstructure from creep, and growth processes, driven by  
 327 the minimisation of surface energy. More abstractly, the equations used to formulate the  
 328 paleowattmeter are based on the notion of stored and dissipated energy which would al-  
 329 low the method to remain valid if the number of dissipative mechanisms was increased  
 330 to include creep cavitation. Additionally, the grain growth equation would need to be  
 331 expanded to include some knowledge of second phases. This could be achieved through  
 332 the integration of the Zener parameter as proposed by Herwegh et al. (2011). The ex-  
 333 act implementation of either of these points is not trivial as it would probably require  
 334 considerable assumption about the partitioning of dissipation or experimental constraints  
 335 on the energetics of creep cavitation at the scale of a sample.

#### 336 4.5 A path from single phase to polyphase

337 While the sample we investigated is considered to be nominally pure, it is clear that  
 338 minor phases are present and mass is being transported during deformation (see fig. 1c  
 339 and d). It is unclear over what distances mass is transported but it is apparent that the  
 340 creep cavities play a role in providing sites of precipitation. The most significant con-  
 341 sequence of this is that, without the aid of chemical reaction or fracture, a monominer-  
 342 alic ductile material has a fundamental and spontaneous path to transition to a second  
 343 phase controlled microstructure and ultimately a polymineralic aggregate.

344 Our results experimentally corroborate the conceptual model of Linckens et al. (2015)  
 345 for ophiolites, where they suggest that a second phase controlled microstructures could

346 arise out of a combination of dynamic recrystallisation and grain boundary sliding. Fur-  
 347 thermore, our results build out the older models of granular flow from Herwegh and Jenni  
 348 (2001) in carbonate shear zones, and more generally the model for mature polyphase shear  
 349 zones of Fussesis et al. (2009). In both cases the nucleation of material occurs, in part,  
 350 because of the production of syn-kinematic pores. The biggest implication of making the  
 351 association with Fussesis et al. (2009) is that we suggest the cavities act as part of a dy-  
 352 namic permeability. Despite the excellent quality of both the experimental and microstruc-  
 353 tural data presented here, we cannot unambiguously show this in our study. That be-  
 354 ing said, our work probably showcases one way that a thoroughly mixed polyphase ul-  
 355 tramylonite can form and points towards important future research questions that in-  
 356 volve creep cavities. In particular: (1) in more chemically complex rocks, does the cou-  
 357 pling of chemistry and mechanics lead to efficient filling of pores?; and (2) if not what  
 358 does this open porosity mean for fault rock stability? We propose that clearly demon-  
 359 strating the true dynamic action of the so called *dynamic granular fluid pump* of Fussesis  
 360 et al. (2009) is one of the next great challenges of our community.

## 361 5 Conclusions and outlook

362 In experiments designed to understand the steady state deformation of deep shear  
 363 zones, we have documented that creep cavities emerge with grain-size reduction by sub-  
 364 grain rotation recrystallisation. This is an important finding because it shows that creep  
 365 driven porosity can be opened and sustained in rocks at a high confining pressure. More  
 366 than this, our results suggest that the transformation of an undeformed monomineralic  
 367 rock into an ultramylonite should be accompanied by syn-kinematic pore formation. A  
 368 direct outcome of this is that, if material is available to precipitate into pores, phase mix-  
 369 tures can form spontaneously from the deformation of single phase rocks. The most provoca-  
 370 tive extension our results is that, if pores remain open, ductile shear zones may neces-  
 371 sarily develop hydro-mechanical anisotropy with ultramylonites providing sites of me-  
 372 chanical instability. More generally, our results challenge the use of grain-size palaeopiezome-  
 373 ters to estimate stress in mylonites as they rely on the assumption that monomineralic  
 374 domains are not affected by precipitation processes.

## 375 Acknowledgments

376 This work was financially supported by the Swiss National Science Foundation (SNSF;  
 377 grant number 162340). We would like to thank Christoph Neururer and Bernard Grob y  
 378 for both their help and the use of their SEM at Fribourg University. James Gilgannon  
 379 would like to thank Alba Zappone for her help in searching through the rock samples  
 380 of ETHZ and Marius Waldvogel for many discussion that helped shape this contribu-  
 381 tion. Supplementary information Datasets can be obtained from the Bern Open Repos-  
 382 itory and Information System (BORIS) under the BORIS doi:10.7892/boris.134751. We  
 383 thank Christian Huber for his role as editor and Alexandre Dimanov, Phil Skemer and  
 384 two anonymous reviewers for their constructive and thorough reviews.

## 385 References

- 386 Akker, I., Kaufmann, J., Desbois, G., Klaver, J., Urai, J., Berger, A., & Herwegh,  
 387 M. (2018). Multiscale porosity changes along the pro- and retrograde deforma-  
 388 tion path: an example from alpine slates. *Solid Earth*, 9(5), 1141–1156. doi:  
 389 <https://doi.org/10.5194/se-9-1141-2018>  
 390 Austin, N., & Evans, B. (2009). The kinetics of microstructural evolution during  
 391 deformation of calcite. *Journal of Geophysical Research: Solid Earth*, 114(B9).  
 392 doi: <https://doi.org/10.1029/2008JB006138>  
 393 Barnhoorn, A., Bystricky, M., Burlini, L., & Kunze, K. (2004). The role of recryst-

- 394 tallisation on the deformation behaviour of calcite rocks: large strain torsion  
 395 experiments on carrara marble. *Journal of Structural Geology*, 26(5), 885 -  
 396 903. doi: <https://doi.org/10.1016/j.jsg.2003.11.024>
- 397 Bercovici, D., & Skemer, P. (2017). Grain damage, phase mixing and plate-boundary  
 398 formation. *Journal of Geodynamics*, 108, 40 - 55. doi: <https://doi.org/10.1016/j.jog.2017.05.002>
- 399
- 400 Bestmann, M., & Prior, D. (2003). Intragranular dynamic recrystallization in natu-  
 401 rally deformed calcite marble: diffusion accommodated grain boundary sliding  
 402 as a result of subgrain rotation recrystallization. *Journal of Structural Geology*,  
 403 25(10), 1597 - 1613. doi: [https://doi.org/10.1016/S0191-8141\(03\)00006-3](https://doi.org/10.1016/S0191-8141(03)00006-3)
- 404 Ceccato, A., Menegon, L., Pennacchioni, G., & Morales, L. (2018). Myrmekite and  
 405 strain weakening in granitoid mylonites. *Solid Earth*, 9(6), 1399–1419. doi:  
 406 <https://doi.org/10.5194/se-9-1399-2018>
- 407 Cross, A. J., & Skemer, P. (2017). Ultramyylonite generation via phase mixing in  
 408 high-strain experiments. *Journal of Geophysical Research: Solid Earth*, 122(3),  
 409 1744–1759. doi: <https://doi.org/10.1002/2016JB013801>
- 410 De Bresser, J., Peach, C., Reijs, J., & Spiers, C. (1998). On dynamic recrystalliza-  
 411 tion during solid state flow: Effects of stress and temperature. *Geophysical Re-*  
 412 *search Letters*, 25(18), 3457–3460. doi: <https://doi.org/10.1029/98GL02690>
- 413 Dimanov, A., Rybacki, E., Wirth, R., & Dresen, G. (2007). Creep and strain-  
 414 dependent microstructures of synthetic anorthite-diopside aggregates. *Journal*  
 415 *of Structural Geology*, 29(6), 1049 - 1069. doi: <https://doi.org/10.1016/j.jsg.2007.02.010>
- 416
- 417 Evans, B., & Kohlstedt, D. (1995). Rheology of rocks. In *Rock physics & phase rela-*  
 418 *tions* (p. 148-165). American Geophysical Union (AGU). doi: <https://doi.org/10.1029/RF003p0148>
- 419
- 420 Fousseis, F., Regenauer-Lieb, K., Liu, J., Hough, R. M., & De Carlo, F. (2009). Creep  
 421 cavitation can establish a dynamic granular fluid pump in ductile shear zones.  
 422 *Nature*, 459, 974977. doi: <https://doi.org/10.1038/nature08051>
- 423 Gilgannon, J., Fousseis, F., Menegon, L., Regenauer-Lieb, K., & Buckman, J. (2017).  
 424 Hierarchical creep cavity formation in an ultramyylonite and implications for  
 425 phase mixing. *Solid Earth*, 8(6), 1193–1209. doi: 10.5194/se-8-1193-2017
- 426 Hackl, K., & Renner, J. (2013). High-temperature deformation and recrystalliza-  
 427 tion: A variational analysis and its application to olivine aggregates. *Journal*  
 428 *of Geophysical Research: Solid Earth*, 118(3), 943–967. doi: <https://doi.org/10.1002/jgrb.50125>
- 429
- 430 Herwegh, M., & Jenni, A. (2001). Granular flow in polymineralic rocks bearing sheet  
 431 silicates: new evidence from natural examples. *Tectonophysics*, 332(3), 309 -  
 432 320. doi: [https://doi.org/10.1016/S0040-1951\(00\)00288-2](https://doi.org/10.1016/S0040-1951(00)00288-2)
- 433 Herwegh, M., Linckens, A., J.and Ebert, Berger, A., & Brodhag, S. (2011). The  
 434 role of second phases for controlling microstructural evolution in polymineralic  
 435 rocks: A review. *Journal of Structural Geology*, 33(12), 1728 - 1750. doi:  
 436 <https://doi.org/10.1016/j.jsg.2011.08.011>
- 437 Hill, R. (1963). Elastic properties of reinforced solids: Some theoretical principles.  
 438 *Journal of the Mechanics and Physics of Solids*, 11(5), 357 - 372. doi: [https://doi.org/10.1016/0022-5096\(63\)90036-X](https://doi.org/10.1016/0022-5096(63)90036-X)
- 439
- 440 Hirth, G., & Tullis, J. (1992). Dislocation creep regimes in quartz aggregates. *Jour-*  
 441 *nal of Structural Geology*, 14(2), 145 - 159. doi: [https://doi.org/10.1016/0191-8141\(92\)90053-Y](https://doi.org/10.1016/0191-8141(92)90053-Y)
- 442
- 443 Kruse, R., Stünitz, H., & Kunze, K. (2001). Dynamic recrystallization processes in  
 444 plagioclase porphyroclasts. *Journal of Structural Geology*, 23(11), 1781 - 1802.  
 445 doi: [https://doi.org/10.1016/S0191-8141\(01\)00030-X](https://doi.org/10.1016/S0191-8141(01)00030-X)
- 446 Lee, K.-H., Jiang, Z., & Karato, S.-I. (2002). A scanning electron microscope study  
 447 of the effects of dynamic recrystallization on lattice preferred orientation in  
 448 olivine. *Tectonophysics*, 351(4), 331 - 341. doi: <https://doi.org/10.1016/>

- 449 S0040-1951(02)00250-0
- 450 Linckens, J., Herwegh, M., & Müntener, O. (2015). Small quantity but large ef-  
 451 fect how minor phases control strain localization in upper mantle shear zones.  
 452 *Tectonophysics*, *643*, 26 - 43. doi: <https://doi.org/10.1016/j.tecto.2014.12.008>
- 453 Lopez-Sanchez, M. A., & Llana-Fúnez, S. (2018). A cavitation-seal mechanism  
 454 for ultramylonite formation in quartzofeldspathic rocks within the semi-  
 455 brittle field (vivero fault, nw spain). *Tectonophysics*, *745*, 132 - 153. doi:  
 456 <https://doi.org/10.1016/j.tecto.2018.07.026>
- 457 Mei, S., Suzuki, A., Kohlstedt, D., Dixon, N., & Durham, W. (2010). Experimental  
 458 constraints on the strength of the lithospheric mantle. *Journal of Geophysical*  
 459 *Research: Solid Earth*, *115*(B8). doi: <https://doi.org/10.1029/2009JB006873>
- 460 Menegon, L., Füsseis, F., Stünitz, H., & Xiao, X. (2015, 03). Creep cavitation bands  
 461 control porosity and fluid flow in lower crustal shear zones. *Geology*, *43*(3),  
 462 227-230. doi: <https://doi.org/10.1130/G36307.1>
- 463 Menegon, L., Stünitz, H., Nasipuri, P., Heilbronner, R., & Svahnberg, H. (2013).  
 464 Transition from fracturing to viscous flow in granulite facies perthitic  
 465 feldspar (lofoten, norway). *Journal of Structural Geology*, *48*, 95 - 112. doi:  
 466 <https://doi.org/10.1016/j.jsg.2012.12.004>
- 467 Michibayashi, K., Ina, T., & Kanagawa, K. (2006). The effect of dynamic recrystal-  
 468 lization on olivine fabric and seismic anisotropy: Insight from a ductile shear  
 469 zone, oman ophiolite. *Earth and Planetary Science Letters*, *244*(3), 695 - 708.  
 470 doi: <https://doi.org/10.1016/j.epsl.2006.02.019>
- 471 Mitchell, E., Kenchington, C., Liu, A., Matthews, J., & Butterfield, N. (2015). Re-  
 472 constructing the reproductive mode of an ediacaran macro-organism. *Nature*,  
 473 *524*, 343 EP -. doi: <https://doi.org/10.1038/nature14646>
- 474 Paterson, M., & Olgaard, D. (2000). Rock deformation tests to large shear strains  
 475 in torsion. *Journal of Structural Geology*, *22*(9), 1341 - 1358. doi: [https://doi.org/10.1016/S0191-8141\(00\)00042-0](https://doi.org/10.1016/S0191-8141(00)00042-0)
- 476
- 477 Pieri, M., Burlini, L., Kunze, K., Stretton, I., & Olgaard, D. (2001). Rheological  
 478 and microstructural evolution of carrara marble with high shear strain: results  
 479 from high temperature torsion experiments. *Journal of Structural Geology*,  
 480 *23*(9), 1393 - 1413. doi: [https://doi.org/10.1016/S0191-8141\(01\)00006-2](https://doi.org/10.1016/S0191-8141(01)00006-2)
- 481 Pieri, M., Kunze, K., Burlini, L., Stretton, I., Olgaard, D., Burg, J.-P., & Wenk,  
 482 H.-R. (2001). Texture development of calcite by deformation and dynamic  
 483 recrystallization at 1000k during torsion experiments of marble to large  
 484 strains. *Tectonophysics*, *330*(1), 119 - 140. doi: [https://doi.org/10.1016/S0040-1951\(00\)00225-0](https://doi.org/10.1016/S0040-1951(00)00225-0)
- 485
- 486 Précigout, J., Prigent, C., Palasse, L., & Pochon, A. (2017). Water pumping in man-  
 487 tle shear zones. *Nature Communications*, *8*(1), 15736. doi: <https://doi.org/10.1038/ncomms15736>
- 488
- 489 Précigout, J., & Stünitz, H. (2016). Evidence of phase nucleation during olivine dif-  
 490 fusion creep: A new perspective for mantle strain localisation. *Earth and Plan-*  
 491 *etary Science Letters*, *455*, 94 - 105. doi: <https://doi.org/10.1016/j.epsl.2016.09.029>
- 492
- 493 Précigout, J., Stünitz, H., & Villeneuve, J. (2019). Excess water storage induced  
 494 by viscous strain localization during high-pressure shear experiment. *Scientific*  
 495 *Reports*, *9*(1), 3463. doi: <https://doi.org/10.1038/s41598-019-40020-y>
- 496 Regenauer-Lieb, K., Karrech, A., Chua, H., Poulet, T., Veveakis, M., Wellmann,  
 497 F., . . . Lester, D. (2014). Entropic bounds for multi-scale and multi-physics  
 498 coupling in earth sciences. In *Beyond the second law: Entropy production and*  
 499 *non-equilibrium systems* (pp. 323-335). Berlin, Heidelberg: Springer Berlin  
 500 Heidelberg. doi: [https://doi.org/10.1007/978-3-642-40154-1\\_17](https://doi.org/10.1007/978-3-642-40154-1_17)
- 501 Stipp, M., Stünitz, H., Heilbronner, R., & Schmid, S. (2002). The eastern tonale  
 502 fault zone: a natural laboratory for crystal plastic deformation of quartz over  
 503 a temperature range from 250 to 700c. *Journal of Structural Geology*, *24*(12),



- 504 1861 - 1884. doi: [https://doi.org/10.1016/S0191-8141\(02\)00035-4](https://doi.org/10.1016/S0191-8141(02)00035-4)
- 505 Ter Heege, J., De Bresser, J., & Spiers, C. (2002). The influence of dynamic re-
- 506 crystallization on the grain size distribution and rheological behaviour of
- 507 carrara marble deformed in axial compression. *Geological Society, Lon-*
- 508 *don, Special Publications*, 200(1), 331–353. doi: [https://doi.org/10.1144/](https://doi.org/10.1144/GSL.SP.2001.200.01.19)
- 509 [GSL.SP.2001.200.01.19](https://doi.org/10.1144/GSL.SP.2001.200.01.19)
- 510 Tullis, J., & Yund, R. (1985, 04). Dynamic recrystallization of feldspar: A mecha-
- 511 nism for ductile shear zone formation. *Geology*, 13(4), 238-241. doi: [https://](https://doi.org/10.1130/0091-7613(1985)13<238:DROFAM>2.0.CO;2)
- 512 [doi.org/10.1130/0091-7613\(1985\)13<238:DROFAM>2.0.CO;2](https://doi.org/10.1130/0091-7613(1985)13<238:DROFAM>2.0.CO;2)
- 513 Twiss, R. J. (1977). Theory and applicability of a recrystallized grain size pale-
- 514 opiezometer. In *Stress in the earth* (pp. 227–244). Basel: Birkhäuser Basel.
- 515 doi: [https://doi.org/10.1007/978-3-0348-5745-1\\_13](https://doi.org/10.1007/978-3-0348-5745-1_13)
- 516 Wiegand, T., Martínez, I., & Huth, A. (2009). Recruitment in tropical tree species:
- 517 Revealing complex spatial patterns. *The American Naturalist*, 174(4), E106-
- 518 E140. doi: <https://doi.org/10.1086/605368>
- 519 Wiegand, T., & Moloney, K. (2014). *Handbook of spatial point-pattern analysis in*
- 520 *ecology*. Boca Raton, FL: Chapman and Hall/CRC.